ADVANCED MATERIALS INTERFACES
www.advmatinterfaces.de

Check for updates

Controlling Atomic Layer Deposition of 2D Semiconductor SnS_2 by the Choice of Substrate

*Miika Mattinen, Peter J. King, Philipp Brüner, Markku Leskelä, and Mikko Ritala**

Semiconducting 2D materials, such as SnS_2, hold great promise in a variety of applications including electronics, optoelectronics, and catalysis. However, their use is hindered by the scarcity of deposition methods offering necessary levels of thickness control and large-area uniformity. Herein, a low-temperature atomic layer deposition (ALD) process is used to synthesize up to 5 × 5 cm² continuous, few-layer SnS_2 films on a variety of substrates, including SiO_2/Si, Si-H, different ALD-grown films (Al_2O_3, TiO_2, and Ir), sapphire, and muscovite mica. As a part of comprehensive film characterization, the use of low energy ion scattering (LEIS) is showcased to determine film continuity, coverage of monolayer and multilayer areas, and film thickness. It is found that on sapphire substrate, continuous films are achieved at lower thicknesses compared to the other substrates, down to two monolayers or even less. On muscovite mica, van der Waals epitaxial growth is realized after the post-deposition annealing, or even in the as-deposited films when the growth is performed at 175 to 200 °C. This work highlights the importance of the substrate choice for 2D materials and presents a practical low-temperature method for the deposition of high-quality SnS_2 films that may be further evaluated for a range of applications.

1. Introduction

2D materials have received immense attention ever since the discovery of the unique and extraordinary properties of semimetallic graphene in 2004.[1] The 2011 report on high-performance field-effect transistors (FETs) based on MoS_2,[2] a semiconducting 2D material, arose interest in MoS_2 and other semiconducting transition metal dichalcogenides (TMDCs). Nowadays, a broad range of 2D materials, including insulators (e.g., h-BN),[3] semimetals (e.g., graphene),[1,4] and metals (e.g., NbS_2),[5,6] have been explored. The 2D semiconductors, such as MoS_2, have become the topic of particularly active research due to the crucial role of semiconductors in modern microelectronics.[7–11]

Tin disulfide (SnS_2) has recently emerged as a highly interesting 2D semiconductor.[12,13] It crystallizes in the CdI_2-type 2D structure (1T phase) similar to many TMDCs[12,14] and has a fairly large, indirect band gap of approximately 2.2 eV in bulk[13,15] and 2.4–2.6 eV as a monolayer.[15,16] SnS_2 has already shown performance comparable to the benchmark 2D semiconductor, MoS_2, in applications such as FETs[9,12,17–19] and photodetectors.[12,20] Furthermore, possible reduction in short-channel leakage[20,21] due to the larger, indirect band-gap of SnS_2 and higher predicted mobility[22] compared to MoS_2 make SnS_2 a favorable material for electronics. Other promising applications for SnS_2 include lithium and sodium-ion batteries,[23,24] gas sensing,[25] and various kinds of catalysis.[26–28]

Synthesis of 2D materials including SnS_2 is, however, a major obstacle for the realization of practical applications. An ideal synthesis method should offer high material quality, monolayer-level thickness control as well as good uniformity on large areas and complex shapes—preferably all at low processing temperatures. The substrate is an integral part of the deposition process and applications, and there are great needs both for methods capable of directly synthesizing 2D materials on different substrates, as well as for methods depositing high-quality materials on single-crystalline substrates. The latter route could be combined with a transfer of the deposited material onto another substrate, if needed.[29–31]

High-quality, few-layer SnS_2 has been produced from bulk crystals by micromechanical exfoliation,[12,17] but this method offers very limited control over the flake size and thickness and has extremely low throughput. Vapor-phase deposition techniques, such as chemical vapor deposition (CVD) and atomic layer deposition (ALD), are promising techniques for the deposition of 2D materials. Thus far, CVD has been mostly used to produce high-quality, isolated few-layer flakes of SnS_2 at 450–700 °C.[16,18,32,33] CVD of continuous SnS_2 films was demonstrated recently, but films below 3–4 nm in thickness remained discontinuous and even 15 nm thick films contained some holes.[34,35] ALD has been used to deposit continuous SnS_2 films with thicknesses from approximately two up to tens of monolayers.[36–41] In addition to thermal ALD processes,[36–39]

Dr. M. Mattinen, Dr. P. J. King,[+] Prof. M. Leskelä, Prof. M. Ritala
Department of Chemistry
University of Helsinki
P.O. Box 55, Helsinki FI-00014, Finland
E-mail: mikko.ritala@helsinki.fi

P. Brüner
IONTOF GmbH
Heisenbergstr. 15, Münster DE-48149, Germany

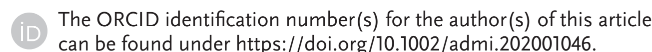
The ORCID identification number(s) for the author(s) of this article can be found under https://doi.org/10.1002/admi.202001046.

[+]Present address: Picosun Oy, Masalantie 365, FI-02430, Masala, Finland

© 2020 The Authors. Published by Wiley-VCH GmbH. This is an open access article under the terms of the Creative Commons Attribution License, which permits use, distribution and reproduction in any medium, provided the original work is properly cited.

DOI: 10.1002/admi.202001046

plasma-enhanced ALD (PEALD) and plasma sulfurization of ALD-grown SnO films have recently been reported as alternative approaches to deposit high-quality SnS_2.[40,41]

ALD is an advanced modification of CVD, which has an unprecedented ability to uniformly coat large and complex, high aspect ratio substrates with atomic level control.[42,43] These advantages stem from the alternate pulsing of precursors, typically one for each film element, which react on the surface in characteristic self-limiting manner. Therefore, uncontrolled gas phase reactions and precursor decomposition are avoided. However, ALD also has certain challenges in the deposition of 2D materials due to the typically low reactivity of ALD precursors on the basal surfaces of 2D materials.[44–46] The growth rates may be low,[44,47,48] rough flake-like films are often obtained,[48–52] and the low growth temperature and high nucleation density lead to small grain size which limits the electrical performance of the films.[38,41,44]

The substrate plays a crucial role in surface-reaction controlled techniques such as ALD and in 2D film growth in general. In addition to the common SiO_2/Si, a range of substrates have been tested for the ALD of 2D materials, such as metal oxides,[44,47,48] gold,[49] carbon fiber paper,[53] polyimide,[41] metal foams,[54] and sapphire.[44,55,56] However, there are few studies comparing film growth on different substrates and, thus, limited understanding on how the substrate affects the film growth and properties. Groven et al.[44] compared amorphous and crystalline (sapphire) Al_2O_3 substrates, and found clear differences in the morphology of WS_2 films grown by PEALD. Notably, they reported that a small fraction of the WS_2 grains oriented epitaxially on sapphire, while the majority of the grains were randomly oriented. Later on, Groven et al.[57] showed that the reactivity of the substrate surface can be used to control the nucleation density and consequently the grain size of the PEALD WS_2 films.

Van der Waals (vdW) epitaxy, a method where a 2D material is grown on a 2D, or even on a suitable 3D substrate, such as sapphire, offers great opportunities for the growth of 2D materials. The absence of covalent bonding between the film and the substrate leads to relaxed requirements on lattice matching compared to the conventional epitaxy and avoids build-up of strain in the films.[58–60] The vdW epitaxially grown nuclei ideally merge together to form a monocrystalline film, which overcomes the limitations of small grain size and thereby improves film properties.[61,62] For SnS_2, vdW epitaxy was demonstrated in the 1990s with films grown in ultra-high vacuum conditions on mica,[63,64] graphite,[65] and various 2D chalcogenides.[63,65] Recently, we demonstrated vdW epitaxy of 2D materials including SnS_2 at low temperatures and in low vacuum conditions using ALD.[66]

Herein, we have prepared air-stable SnS_2 thin films on different substrates by ALD using tin(IV) acetate and hydrogen sulfide at 150 °C followed by mild H_2S/N_2 annealing at 250–300 °C to crystallize the films.[36] This process has been shown to deposit continuous, high-quality SnS_2 films from approximately two to ten monolayers in thickness on SiO_2/Si substrates. We show that crystalline SnS_2 films can be successfully grown on a variety of substrates with clear differences in film continuity, morphology, and crystallinity. For example, on sapphire, continuous films are obtained at lower thicknesses than on the other substrates, such as SiO_2/Si. On muscovite mica, vdW epitaxial growth is observed and either smooth and continuous films or triangular crystallites are obtained depending on the deposition conditions.

2. Results and Discussion

2.1. Overview of Growth and Crystallinity on Different Substrates

In this study, we illustrate how the substrate can affect the growth, morphology, continuity, and crystallinity of SnS_2 films deposited by ALD using tin(IV) acetate [$Sn(OAc)_4$] and hydrogen sulfide (H_2S) precursors at 150 °C followed by post-deposition annealing at 250–300 °C in a H_2S/N_2 atmosphere.[36] More details on the film deposition and substrates used can be found in Section 4. In this section, we begin by comparing film growth and crystallinity on a wide range of substrates. The following sections will concentrate on films grown on single-crystalline sapphire (Section 2.2.) and mica (Section 2.3.). Unlike the typical silicon substrates with an amorphous SiO_2 layer (denoted SiO_2/Si), these two substrates can help direct and stabilize SnS_2 films due to the similarities in atomic arrangement and symmetry of the substrates and SnS_2. The differences between the substrates are then shown to become even clearer at higher deposition temperatures (Section 2.4.). Finally, in Section 2.5, we present a summary of the results and insights obtained in this study. Supporting Information contains additional results and in-depth discussion on factors affecting film growth and crystallinity such as the surface and interface energies, the structure of the substrate surfaces and the reactive sites present, the interfaces formed, and the interplay of kinetic and thermodynamic effects.

First, we observed that crystalline SnS_2 films could be obtained after annealing on all of the tested substrates except for Ge-H (**Figure 1**a; Figure S1, Supporting Information), as is evident from the presence of the (0001)SnS_2 reflection close to the expected position of 15.0° 2θ (JCPDS-ICDD PDF 26–0677). We examined the out-of-plane orientation of the films using α scans (section of an in-plane pole figure at an arbitrary rotation β), where $\alpha = 90°$ corresponds to planes parallel to the substrate surface and $\alpha = 80°$, for example, to planes tilted by 10° with respect to the surface. Compared to the native-oxide covered silicon (SiO_2/Si), stronger (0001) texture was observed on mica, sapphire, ALD-Al_2O_3, and Si-H substrates (Figure 1b; Figure S2a, Supporting Information). Sapphire and mica were chosen for more detailed investigations because the films deposited on ALD-Al_2O_3 and Si-H were found to be rough (Figure S3, Supporting Information) and the thinnest films on Si-H exhibited poor (0001) texture (Figure S2b, Supporting Information). The lack of crystallinity in the thinnest films on Si-H as well as in all of the films on Ge-H may be due to an interfacial reaction between the film and the substrate resulting in formation of an amorphous silicide or germanide.

Substrate-enhanced growth,[36] in other words an initial period of faster growth followed by slower, linear growth at approximately 0.1 Å $cycle^{-1}$ was observed on the SiO_2/Si, thermal SiO_2, Si-H, sapphire, and mica substrates (Figure 1c). The only major difference was the faster initial growth up to 100 cycles on mica, whereas the growth during the following cycles was slower on mica compared to the other substrates. This is suggested to be due to differences in nucleation as

 © 2020 The Authors. Published by Wiley-VCH GmbH

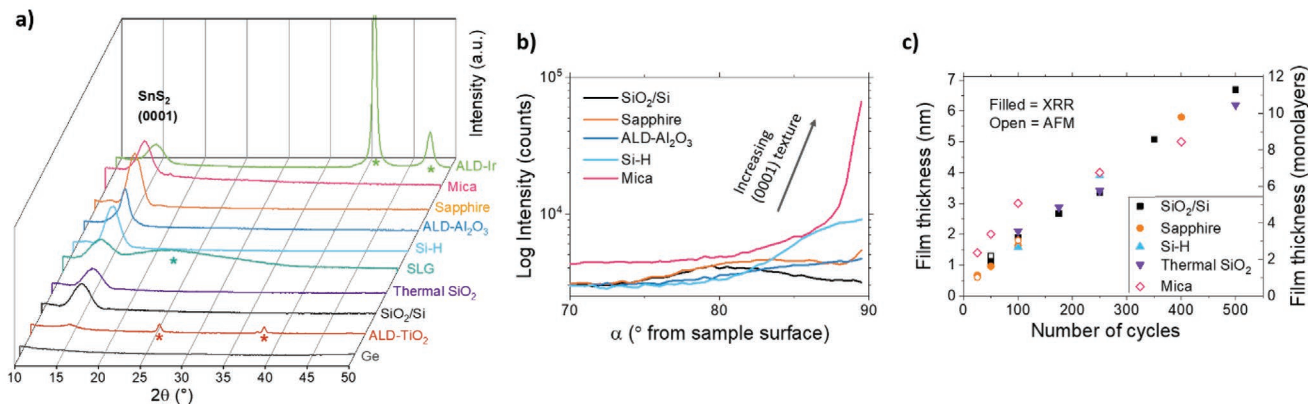

Figure 1. Growth of SnS_2 films on different substrates. a) Grazing incidence X-ray diffractograms (asterisks denote reflections originating from the substrates), b) α scans of the (0001)SnS_2 reflection, and c) thickness of annealed SnS_2 films deposited on different substrates. Unless otherwise noted, the films were deposited at 150 °C using 250 cycles and annealed at 250 °C in a H_2S/N_2 atmosphere.

well as structure and reactivity of the as-grown (mainly amorphous) films.

Some differences in the crystallization during the film growth on the different substrates were also observed. On ALD-Al_2O_3, for example, some crystallinity was detected already after 250 ALD cycles, whereas the films grown on SiO_2/Si remained amorphous even after 400 cycles (Figures S4 and S5, Supporting Information). After annealing, crystallization was observed for all of the films deposited on different substrates with a varying number of ALD cycles (25–500), except for those deposited on Ge-H and the thinnest films (≤50 cycles) on Si-H as discussed above.

2.2. Films Grown on Sapphire

Next, the films grown on single-crystalline sapphire (α-Al_2O_3), a substrate commonly used for the growth of TMDCs due to its hexagonal structure, are discussed in more detail. Prior to the film deposition, the 2″ c-plane sapphire wafers were annealed in air at 1000 °C for 2 h to create a hexagonal surface consisting of atomically smooth (0001) terraces separated by steps with a height of approximately 2 Å.[67,68] The pre-treatment improved film crystallinity and smoothness (Figures S6 and S7, Supporting Information), as was reported earlier for the growth of MoS_2 on sapphire.[61] The thinnest films deposited using 25–100 cycles on sapphire were notably (0001) textured after annealing the films at 250 °C as shown by the α scans (**Figure 2**a) and θ–2θ X-ray diffractograms (Figure S8, Supporting Information). In thicker films, a large part of the grains were tilted by ≈10° ($\alpha \approx 80°$) with respect to the substrate, which is similar to the films grown on SiO_2/Si.[36]

The SnS_2 films deposited on sapphire remained smooth after the annealing, as evidenced by the low roughness values and visibility of the 2 Å high sapphire steps in atomic force microscopy (AFM) images (Figure S9, Supporting Information). Even the thinnest film deposited using 25 cycles crystallized upon annealing, as shown by in-plane X-ray diffraction (XRD) (Figure 2b; Figure S10, Supporting Information). In-plane XRD detects planes perpendicular to the substrate, and is thus less affected by the very low film thickness that causes peak broadening and a strong decrease of intensity in conventional out-of-plane XRD measurements (see the GIXRD and θ–2θ diffractograms in Figure S8, Supporting Information). Additionally, in the out-of-plane measurements the (0001) peak shifted to smaller angles with decreasing film thickness, which seems to imply an increased interlayer spacing. No shifts were observed in the in-plane measurements, showing that the in-plane lattice spacing remained unchanged when the film thickness was varied.

The appearance of only the $(10\overline{1}0)$ and $(11\overline{2}0)$ reflections in the in-plane diffractograms supports the out-of-plane (0001) texture, as these planes are perpendicular to the (0001) basal planes oriented parallel to the substrate. On the other hand, the simultaneous detection of both the $(10\overline{1}0)$ and $(11\overline{2}0)$ reflections in a $2\theta\chi$ measurement suggests random in-plane orientation, in other words lack of an epitaxial relationship between the film and the substrate, which was further confirmed by in-plane ϕ scans (not shown). Previously, vdW epitaxy of 2D materials on sapphire has been achieved with CVD-grown MoS_2,[61,69] for example. However, the vdW epitaxy on sapphire appears to be rather sensitive to the precise experimental conditions, as some groups have found no signs of epitaxy even when using the same CVD precursors.[70,71] Also, we were unable to achieve epitaxial growth of ALD-grown TMDCs HfS_2, MoS_2, ReS_2, and ZrS_2 on sapphire at temperatures ranging from 250 to 400 °C.[66] It is worth noting that qualitatively, there is a similar hexagonal arrangement of both oxygen and aluminum atoms in sapphire (rhombohedral, space group 167, $R\overline{3}c$, JCPDS-ICDD 46–1212) and sulfur atoms in SnS_2 (trigonal, space group 164, $P\overline{3}m1$, JCPDS-ICDD 26–677). Their lattice constants are markedly different (3.65 and 4.76 Å for SnS_2 and sapphire), although this is not necessarily a problem for vdW epitaxy. Also, it is known that the surface termination of sapphire is sensitive to preparation conditions as is discussed in Section S8 (Supporting Information). It is possible that a hydroxylated surface formed upon exposure to air may not be as efficient a template for epitaxial growth as a bare, clean sapphire surface would be.

According to AFM (Figure 2c) even the thinnest annealed SnS_2 film (25 cycles) on sapphire seemed to be continuous, and its apparent thickness measured across a scratch corresponded to a single SnS_2 monolayer (nominally 5.9 Å). The slightly increased roughness of the 25 cycle SnS_2 film compared to the bare sapphire substrate (Figure 2c) suggests the presence

© 2020 The Authors. Published by Wiley-VCH GmbH

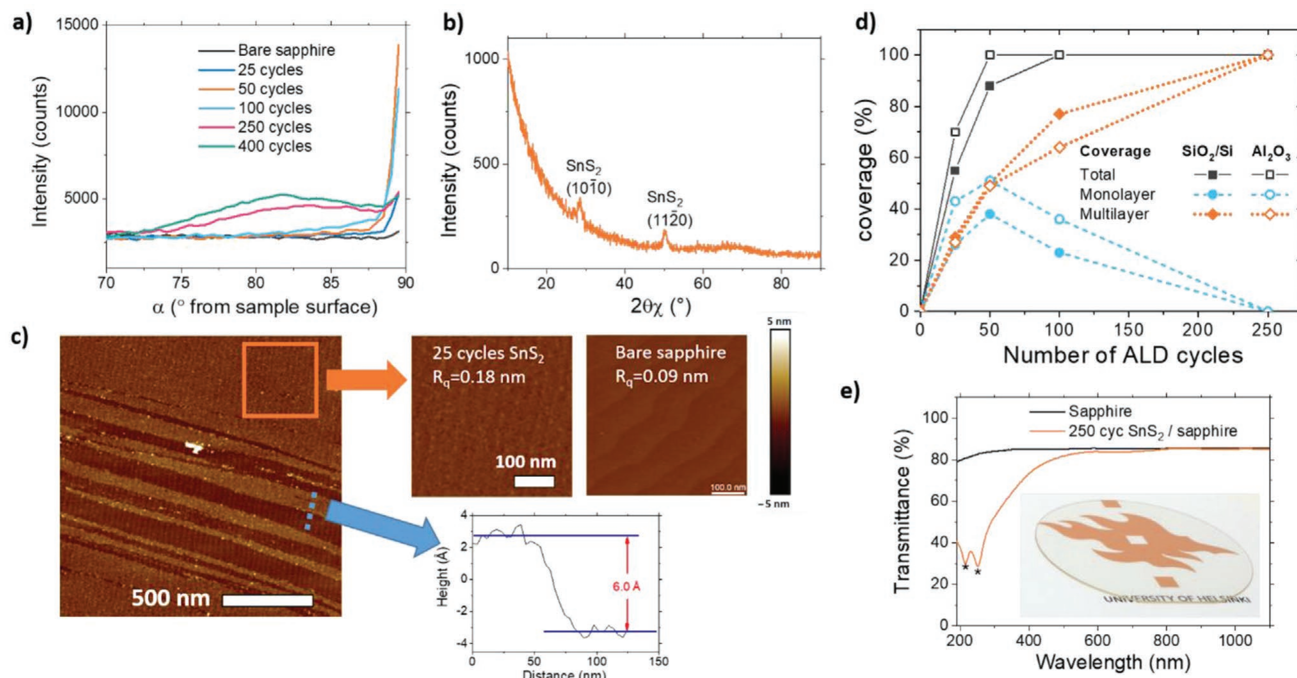

Figure 2. SnS_2 films grown on sapphire. a) α scans of the (0001)SnS_2 reflection of films of different thicknesses. b) In-plane X-ray diffractogram ($2\theta\chi$ scan) of an annealed SnS_2 film deposited on sapphire using 25 cycles. c) AFM image of an annealed 25 cycle film on sapphire after gentle scratching. Insets show the roughness of the film and bare sapphire substrate as well as an averaged line drawn over the film edge (approximate position marked on the AFM image with a dashed line). d) Coverage of SnS_2 films on sapphire (Al_2O_3) and SiO_2/Si as determined by LEIS. e) UV–vis transmittance spectra of bare and SnS_2-coated (250 cycles, annealed) 2” sapphire wafers with a photograph of the latter as inset. All of the films were annealed at 250 °C after deposition.

of local thickness variations. In contrast, a 25 cycle SnS_2 film grown on SiO_2/Si was smooth as deposited, but became clearly discontinuous after the annealing.[36]

Low energy ion scattering (LEIS) measurements on the annealed 25–250 cycle films were performed to assess film coverage as a function of film thickness. In addition to the SnS_2 films on sapphire, films deposited on SiO_2/Si were examined for comparison. The coverage of the thinnest films on sapphire was clearly increased compared to SiO_2/Si. Full coverage on sapphire was reached after 50 cycles compared to 100 cycles on SiO_2/Si (Figure 2d, see Figures S11 and S12, Supporting Information for the data). Furthermore, careful analysis of the data allowed us to break the coverage down into the coverage of monolayer and multilayer SnS_2 as explained in the Experimental Section and illustrated in Figure S13, Supporting Information. It is clear that not only the total coverage but also the monolayer coverage was higher on sapphire than on SiO_2/Si. The monolayer coverage was at its highest after 50 cycles and monolayer areas were still observed in 100 cycle SnS_2 films that completely covered both of the substrates.

LEIS can also be used to estimate the thickness of the film, or in case of sub-100% coverage, height of the islands. The analysis suggests that in the 25 cycle sample on sapphire, for example, approximately 43% was covered by a monolayer of SnS_2, 27% by multilayer areas with an average thickness of 1.2 nm (two SnS_2 monolayers), and 30% of the area exposed the bare sapphire surface.

LEIS and AFM suggested somewhat different levels of film coverage for the thinnest films. For example, according to AFM, the 25 cycle film on sapphire and the 50 cycle film on SiO_2/Si seemed to fully cover the substrate but according to LEIS they only had coverages of 70% and 88%, respectively. A possible explanation is that the AFM tip (diameter ≈ 20 nm) is unable to see small, nanometer-scale holes in the SnS_2 films. Also, the analysis area of AFM is several orders of magnitude smaller compared to LEIS (a few µm^2 compared to a few mm^2, respectively). Nevertheless, AFM images recorded from different areas of the samples were found to be identical.

The average thicknesses of the thinnest continuous films were 1.0 and 1.9 nm on sapphire (50 cycles) and SiO_2/Si (100 cycles), as measured by X-ray reflectivity (XRR), which correspond to slightly below two and approximately three monolayers of SnS_2. For films with local thickness variations, LEIS can be used to obtain more detailed thickness information. For the 50 cycle film on sapphire, LEIS suggests that 51% was covered by monolayer and 49% by multilayers with an average thickness of 1.4 nm. For the 100 cycle film on SiO_2/Si, 23% was covered by a monolayer and 77% by SnS_2 multilayers (average thickness 1.8 nm). Nevertheless, despite these suggested thickness variations, AFM showed the films to be smooth (Figure S9, Supporting Information). For thicker films deposited using 100 cycles or more, LEIS thicknesses were in a good agreement with the other methods, such as AFM, ellipsometry, transmission electron microscopy (TEM), and XRR (Figures S14–S16, Supporting Information).

© 2020 The Authors. Published by Wiley-VCH GmbH

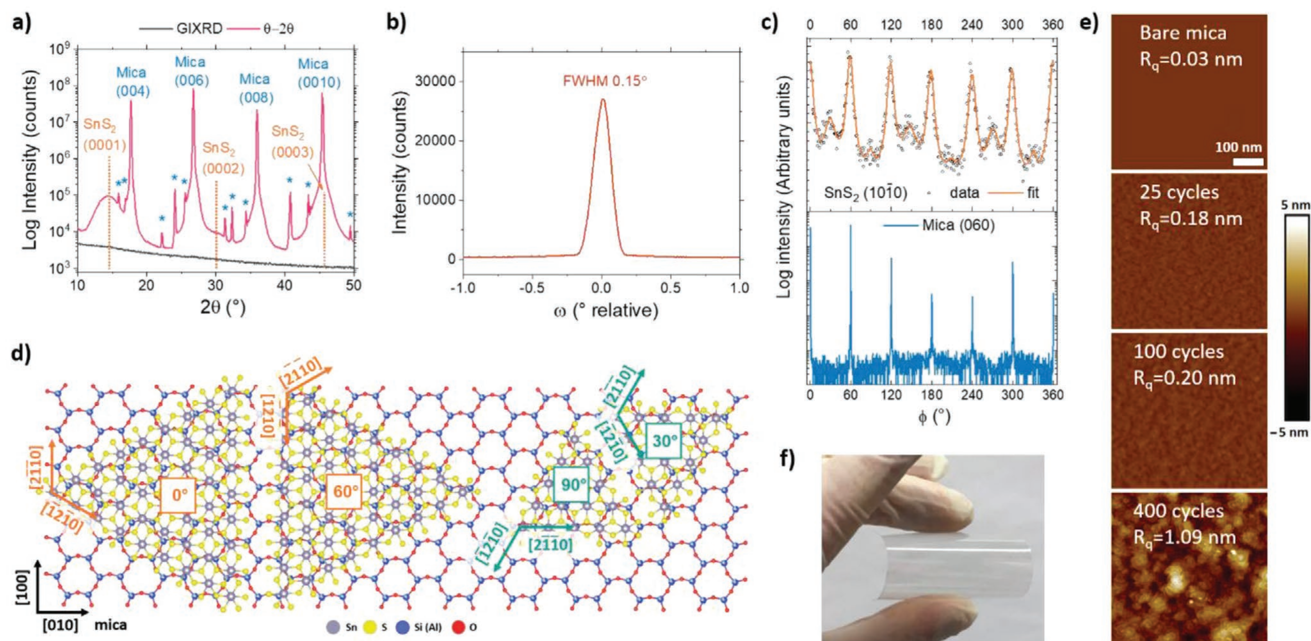

Figure 3. SnS_2 films on mica. a) Grazing incidence and θ–2θ X-ray diffractograms (blue asterisks mark substrate peaks from W Lα and Cu Kβ radiation, see Section 4), b) rocking curve of the (0001)SnS_2 reflection and c) in-plane ϕ scans of the (10$\bar{1}$0)SnS_2 and (060)mica reflections of a 250 cycle SnS_2 film deposited on mica and annealed at 300 °C. d) Schematic illustration of SnS_2 orientations on mica. For clarity only the topmost layer of mica (K^+ ions are omitted) and one S-Sn-S layer of SnS_2 are shown. e) AFM images of bare mica and SnS_2 films of different thicknesses after annealing at 250 °C. f) Photograph of a SnS_2 film deposited on a 5 × 5 cm^2 mica substrate bent to a radius of approximately 1 cm.

The SnS_2 films were visually uniform on 2″ sapphire wafers and exhibited high transmittance in visible and near-IR wavelengths (Figure 2e). The decreased transmittance below 500 nm is attributed to absorption due to the indirect gap of SnS_2, which is reported to be 2.2 eV (≈560 nm) for bulk SnS_2 and approximately 2.4–2.6 eV (≈520–480 nm) for a monolayer of SnS_2.[13,15,16,72] The two distinct minima in transmittance near 250 nm (≈5.0 eV) and 215 nm (≈5.8 eV) result from transitions between specific valence and conduction band states and have also been observed in bulk SnS_2 crystals,[72,73] which supports the high quality of our SnS_2 films.

2.3. Films Grown on Muscovite Mica

Next, we turn our attention to the films deposited on muscovite mica, a layered (2D) potassium aluminosilicate mineral [$KAl_2(Si_3Al)O_{10}(OH)_2$]. An atomically flat mica surface[74] was prepared by cleaving a sheet of muscovite mica (up to 5 × 5 cm^2) immediately before deposition. Muscovite mica cleaves along the potassium layer exposing a (001) surface with Si (one in four substituted by Al) and O atoms arranged in a pseudo-hexagonal structure (Figure S31, Supporting Information),[74–76] which resembles the hexagonal bottom sulfur layer of SnS_2. Half of the potassium ions remain on each cleaved surface. SnS_2 films deposited on mica were found to have a strong (0001) out-of-plane texture after the H_2S/N_2 annealing, as evidenced by the presence of only (0001)SnS_2 and (001)mica peaks in the θ–2θ X-ray diffractogram that shows planes parallel to the substrate and the lack of any peaks in the grazing incidence diffractogram that only shows planes that are tilted with respect to the substrate (**Figure 3**a). The (0001) texture was quantified by a rocking curve XRD measurement of the (0001)SnS_2 reflection, which resulted in a narrow peak with a full-width at half-maximum (FWHM) of ≈0.15° (Figure 3b). The thinnest films deposited using <100 cycles had the strongest texture as evidenced by the rocking curve measurements (Figure S17, Supporting Information). Annealing the films at a higher temperature of 300 °C (compared to 250 °C) further strengthened the out-of-plane texture and decreased the roughness of the SnS_2 films on mica. In comparison, annealing the films deposited on sapphire and SiO_2/Si at 300 °C increased the roughness and did not improve the out-of-plane texture of SnS_2 films and at 350 °C formation of Sn_2S_3 and/or SnS was observed (Figures S23 and S24, Supporting Information). Annealing the SnS_2 films on mica at 325 °C also caused the crystalline quality and morphology of SnS_2 to deteriorate (Figures S18–S20, Supporting Information). Therefore, annealing at 300 °C was deemed optimal for the films on mica (250 °C on SiO_2/Si and sapphire).

In addition to the out-of-plane (0001)SnS_2 ∥ (001)mica registration, preferred in-plane orientation was observed in the SnS_2 films grown on mica, which suggests vdW epitaxial growth in agreement with our previous studies.[66] In-plane ϕ scans of the (060)mica and (10$\bar{1}$0)SnS_2 reflections both resulted in six peaks separated by 60°. These peaks were observed at the same ϕ angles (Figure 3c). Additionally, six weak peaks at a 30° rotation with respect to the stronger peaks (i.e., at 30, 90, 150, 210, 270, and 330 °ϕ) were observed for the (10$\bar{1}$0)SnS_2 reflection. Although SnS_2 (trigonal, space group 164, $P\bar{3}m1$, JCPDS-ICDD 26–0677) has three-fold rotational symmetry around the c-axis, the (10$\bar{1}$0)SnS_2 plane has six-fold rotational symmetry, which results in six peaks at 60° intervals from a single SnS_2

 © 2020 The Authors. Published by Wiley-VCH GmbH

orientation. The observation of six peaks in the (060)mica ϕ scan is attributed to the presence of different stacking orientations in mica,[77] which combined with the mirror symmetry of mica results in two peaks separated by 180° from each of the three stacking orientations (0, 60, and 120°) for a total of six peaks at 60° intervals.

Therefore, the in-plane XRD measurements suggest that mainly the $[2\bar{1}\bar{1}0]$ or $[1\bar{2}10]$ directions of SnS_2 are oriented along the [100]mica direction in-plane. The second orientation corresponds to a 60° rotation with respect to the first orientation, which is expected due to the mirror symmetry of the muscovite mica surface (monoclinic, space group 15, *C*2/*c*, JCPDS-ICDD PDF 72–1503).[78] The peaks in the $(10\bar{1}0)SnS_2$ ϕ scans were relatively wide with FWHM of ≈10°, which indicates rotational disorder, whereas the (060)mica peaks were sharp (FWHM ≈ 0.5°). The minority 30/90° orientations correspond to the alignment of $[1\bar{1}00]SnS_2$ or $[0\bar{1}10]SnS_2$ parallel to [100]mica, the two orientations also being related by a 60° rotation. The suggested SnS_2/mica orientations are illustrated in Figure 3d. Although the lattice constants of SnS_2 (3.65 Å) and mica (5.52 Å approximated as hexagonal) are quite different, the observed epitaxial growth can be rationalized using the coincidence site lattice or domain matching epitaxy concept.[79–81] A 7 × 7 supercell of SnS_2 has only a 1.5% lattice mismatch when compared to a 5 × 5 supercell of mica, if the mica surface is approximated as hexagonal (Figure S21, Supporting Information).[66] The same 0/60° and 30/90° orientations have been observed for several vdW epitaxial systems,[66] including molecular beam epitaxy-grown SnS_2 on mica.[64]

AFM showed the bare mica surface to be atomically smooth. The as-deposited and annealed films were also smooth up to 100 cycles, whereas the films deposited using 250 or more cycles exhibited clearly increased roughness (Figure 3e; Figure S22, Supporting Information). The increased roughness of the thicker films may be due to formation of crystalline nuclei already during the film growth, which can then continue to grow and reach above the surrounding film surface both during growth and annealing. Alternatively, there may be a build-up of strain during film growth. Upon annealing, the release of this strain may result in a roughened surface. The epitaxial film/substrate registration and possible defects and dislocations may also have an effect on the morphology.

Muscovite mica exhibits high transparency and flexibility at thicknesses below about 100 and 10 µm, respectively.[76] The transparency and flexibility were retained after the deposition of SnS_2 films on up to 5 × 5 cm^2 mica substrates, as shown in Figure 3f. We believe that these attributes combined with the good dielectric properties of mica[76] make the epitaxial SnS_2/mica system interesting for applications such as flexible electronics and optoelectronics.

2.4. Effect of Deposition Temperature

Increasing the deposition temperature by only 25 °C (from 150 to 175 °C) led to formation of epitaxial SnS_2 films on mica without post-deposition annealing. A sample deposited using 500 cycles consisted of triangular grains with lateral sizes up to 300 nm and heights from about 2 to 10 nm. The vdW epitaxial growth with 0° and 60° as well as 30° and 90° domains present, is apparent already from the orientation of the domains (**Figure 4**a) and was further confirmed by the in-plane ϕ scan measurements showing epitaxial alignment with in-plane disorder (Figure S25, Supporting Information). The triangular grains were either pyramidal with steps of mostly one or two monolayers in height (1 ML = 0.59 nm), or flat-topped with a height of a few monolayers (Figure 4b).

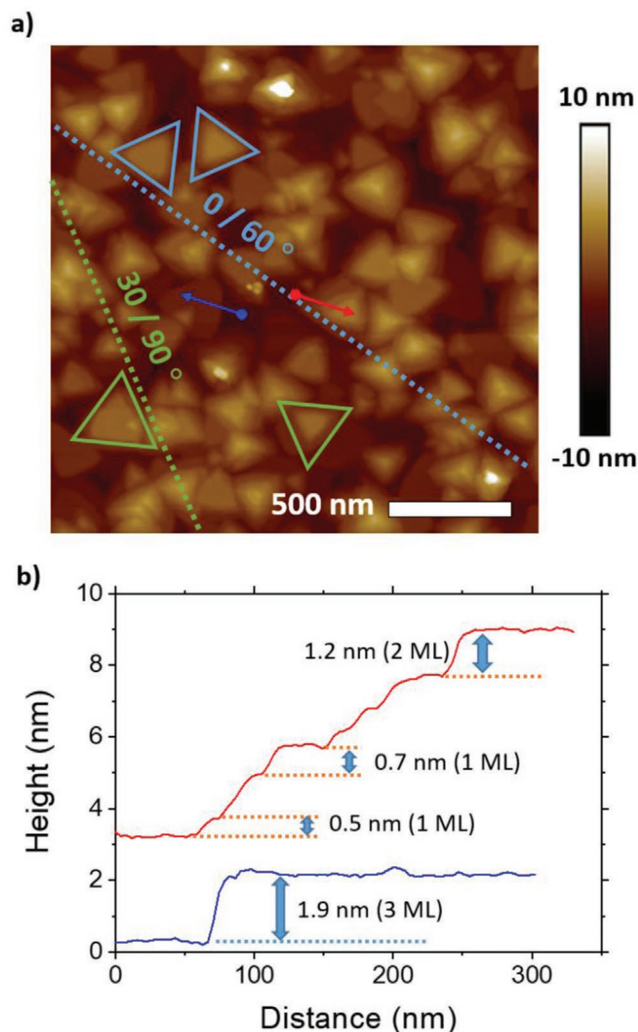

Figure 4. SnS_2 films deposited on mica at 175 °C. a) AFM image of an as-deposited SnS_2 film (175 °C, 500 cycles) on mica. The triangles and dashed lines illustrate the major orientations. The blue and red arrows show the positions of the sections shown in (b). b) Sections drawn over representative flat-topped (blue) and stepped pyramidal (red) grains in (a).

Annealing the films deposited on mica at 175 °C had a detrimental effect on their crystallinity and morphology (Figures S26 and S27, Supporting Information). Furthermore, films with a fairly similar morphology, but with a smaller surface coverage of the triangular grains could be deposited on mica at 200 °C. At this temperature, however, the edges of the grains became more jagged and irregular (Figure S28, Supporting Information). At even higher temperatures, no film growth took place on mica.

© 2020 The Authors. Published by Wiley-VCH GmbH

Deposition temperatures above 150 °C led to completely different morphologies on the other substrates. At 175 °C, only a few flakes and tens of nanometers tall pyramidal grains standing up from the surface were formed on SiO_2/Si, possibly on top of an amorphous SnS_2 layer. On sapphire, a rough, polycrystalline (non-epitaxial) SnS_2 film was deposited (Figure S29, Supporting Information). At 200 °C, no film growth took place on SiO_2/Si or sapphire, which supports the stabilizing effect of the vdW interactions on the growth of SnS_2 on mica.

2.5. Comparison of SnS_2 Films on Different Substrates

In order to facilitate easy comparison of film growth, crystallinity, and continuity on different substrates, the main findings of the study are summarized in **Table 1**. Obviously, clear differences were observed in all of the aforementioned aspects. Possible reasons behind the observations are many and they are discussed in detail in Section S8 of the Supporting Information. These include the surface and interface energies of the substrates and SnS_2, the structure of the substrate surfaces in the deposition conditions and the reactive sites present, the type of interfaces formed, strain, and the interplay of kinetic and thermodynamic effects, for example. Unfortunately, the lack of relevant data on energetics in the literature and the complex nature of the studied systems prevents us from drawing definite conclusions.

Regarding film growth, the main difference was the faster growth on mica up to 100 cycles after which the growth slowed down compared to SiO_2/Si, thermal SiO_2, Si-H, and sapphire. The differences may be attributed to the density and type of functional groups present on the different substrates. While there are abundant reactive hydroxyl groups on the SiO_2 and sapphire surfaces, the reactive sites on hydrogen-terminated silicon are likely Si-H bonds. On mica, either buried −OH groups or bridging Si-O-Si moieties may react with the precursors.

After the annealing, the improved crystal quality on mica, and to a smaller degree on sapphire, compared to SiO_2/Si was also apparent in the increase of the average domain (crystallite) size estimated using the Scherrer equation on in-plane XRD data. The domain size increased from 14 nm on SiO_2/Si to 70 nm on mica for 5 nm thick SnS_2 films. However, considering the in-plane disorder and presence of four SnS_2 rotational domains in the vdW epitaxial films on mica, it is clear that further improvements in film quality on mica are possible.

The thinnest continuous films, approximately 2 ML thick according to LEIS, could be prepared on sapphire. On oxide-terminated silicon, approximately 3 ML thick films at minimum were continuous. Noting that AFM suggested an earlier closure of films compared to LEIS, the minimum thickness for continuous films seemed to be slightly higher on mica than on SiO_2/Si. The differences between these analysis methods, as discussed in Section 2.3., are interesting and warrant further study considering that AFM is the most commonly method in the literature. The differences in continuity between different substrates are a result of a complex interplay of many factors as discussed in the Supporting Information (Section S8, Supporting Information). While complete understanding of all factors affecting continuity are currently out of reach, studies on the effects of different substrate treatment procedures, for example, would be interesting in the future.

Finally, increasing the deposition temperature to 175–200 °C provided additional evidence for the beneficial effects of mica on the crystallinity of SnS_2. On mica, epitaxial SnS_2 films consisting of triangular grains up to 300 nm in width were grown without annealing, which is among the largest grain sizes observed for ALD-grown TMDCs.[82] In contrast, very rough (175 °C) or no films (200 °C) were observed on SiO_2/Si and sapphire.

3. Conclusion

We deposited continuous few-layer SnS_2 films on a variety of substrates by a low-temperature ALD process, followed by mild H_2S/N_2 annealing at 250–300 °C to crystallize the mainly amorphous as-deposited films. The film growth at 150 °C proceeded with a similar growth rate on SiO_2/Si, Si-H, and sapphire, whereas on mica the growth was initially faster and then slower compared to the other substrates. More dramatic

Table 1. Summary of SnS_2 growth, continuity, and crystallinity on different substrates. * = ALD-grown films on silicon, – = not studied. Unless otherwise noted, the results refer to films grown at 150 °C followed by H_2S/N_2 annealing at 250 °C (300 °C for films on mica). The average domain (grain) sizes were determined for 5 nm thick films using in-plane XRD as reported in ref. [66].

Substrate	Crystallinity (domain size)	Minimum continuous thickness	Notes	Growth at higher T_{dep}
SiO_2/Si	<3 ML (0001) texture ≥3 ML weak (0001) texture (domain size ≈14 nm)	≈3 ML (LEIS) ≈2 ML (AFM)	Substrate has native oxide	175 °C: few flakes 200 °C: no growth
Sapphire	≤3 ML strong (0001) texture >3 ML weak (0001) texture (domain size ≈23 nm)	≈2 ML (LEIS) ≈1 ML (AFM)	Substrate pre-annealing beneficial	175 °C: rough film 200 °C: no growth
Mica	vdW epitaxy: Strong (0001) texture for all thicknesses. Likely four domains with disorder (domain size ≈70 nm)	≈3 ML (AFM)	≤100 cycles growth faster vs. Si and sapphire, >100 cycles slower	175–200 °C: vdW epitaxial as deposited (triangular grains)
Thermal SiO_2, SLG	Similar to SiO_2/Si	–	Growth similar to silicon	–
Si-H, Al_2O_3*	Slightly stronger (0001) texture vs. SiO_2/Si	–	Films rough (crystallization during growth)	–
Ir,* TiO_2*	Weak (0001) texture	–	Rough substrates	–
Ge-H	No crystallization	–	Reaction with Ge?	–

© 2020 The Authors. Published by Wiley-VCH GmbH

differences were seen in the crystallinity and morphology of the films. After annealing, polycrystalline SnS_2 films with a relatively weak (0001) texture were obtained on most of the tested substrates including SiO_2/Si, Si-H, and different ALD films (Al_2O_3, Ir, TiO_2). The films deposited on sapphire were more strongly textured and fully covered the substrate at a smaller thickness compared to SiO_2/Si. According to a detailed LEIS analysis, the thicknesses of the thinnest continuous SnS_2 films were approximately two and three monolayers on sapphire and SiO_2/Si, although local thickness variations were observed on both substrates. On mica, vdW epitaxial growth with a very strong (0001) out-of-plane texture, four rotationally different domains, and large in-plane disorder was observed. Using a higher deposition temperature of 175–200 °C, triangular grains up to 300 nm in width with epitaxial registration could be grown on mica without post-deposition annealing. We believe that the deposition of SnS_2 films by ALD with improved continuity and crystallinity on wafer-scale sapphire and mica substrates is an important step towards the use of SnS_2 in applications such as (flexible) electronics and optoelectronics.

4. Experimental Section

Film Deposition: SnS_2 films were deposited using a commercial hot-wall, cross-flow type ALD reactor (F120, ASM Microchemistry) using tin(IV) acetate [Sn(OAc)$_4$] and hydrogen sulfide (H_2S) as precursors.[36] Sn(OAc)$_4$ (Alfa Aesar) was evaporated from an open glass boat held at 130 °C inside the reactor and pulsed by inert gas valving. Sn(OAc)$_4$ is air and moisture sensitive and was handled in a glove box under nitrogen until it was transferred into the reactor. H_2S (Linde, 99.5%) was supplied through needle and solenoid valves at a flow rate of 14 sccm. The films were deposited at 150 °C unless otherwise noted using 1 s Sn(OAc)$_4$ and 4 s H_2S pulses separated by 2 s N_2 purges. This ALD cycle was repeated 25–500× to deposit films of desired thickness. Nitrogen (N_2, AGA, 99.999%) at a flow rate of 400 sccm was used as a carrier and purge gas at a pressure of approximately 5 mbar. Unless otherwise noted, the films were annealed in the ALD reactor under flowing N_2 (400 sccm) mixed with H_2S pulses (14 sccm) for 1 h at 250 °C. H_2S was supplied in 3 s pulses with 0.5 s N_2 purge between the pulses to avoid overheating the pulsing valves.

Substrate Preparation: Various substrates with sizes up to 5 × 5 cm^2 were used: silicon (100) with native oxide layer (denoted SiO_2/Si), 90 nm thermal SiO_2 on Si(100) (denoted thermal SiO_2), soda lime glass (SLG), ALD films (Al_2O_3, TiO_2, and Ir) on silicon, hydrogen-terminated Si and Ge (Si-H and Ge-H), c-plane sapphire, and muscovite mica. Silicon pieces were cut from 6 or 8″ wafers (Okmetic) and blown clean using pressurized N_2. The native silicon oxide was not removed, thus the substrate is denoted SiO_2/Si. SLG was cleaned by successive ultrasonic baths in alkaline ultrasonic cleaning solution (Branson industrial strength cleaner), tap H_2O, ethanol, and deionized H_2O, rinsed with a 50:50 v/v-% solution of ethanol and deionized water, and finally blown dry using pressurized air. Thermal SiO_2 and the previously deposited ALD films were cut to suitable size and blown clean with pressurized N_2. Si-H and Ge-H were prepared by dipping the substrates into 1 v-% aqueous HF for 2 min, followed by careful rinsing with deionized H_2O. Sapphire wafers (2″ wafers, c-plane off to M-plane by 0.2±0.1°, double-side polished, University Wafer) were rinsed with ethanol, acetone, and isopropanol and blown dry using N_2, followed by annealing in a muffle oven in air at 1000 °C for 2 h to create flat (0001) terraces separated by atomic steps.[67,68] Muscovite mica sheets (Nano-Tec, V1 grade, 2.5 × 5 or 5 × 5 cm^2, 0.15–0.21 mm thickness) were cleaved immediately before deposition using a double-edge razor blade to create a fresh, silica-terminated (001) surface.[74] The mica substrates easily bent or cleaved unevenly, which resulted in great difficulties in aligning the samples for the XRD measurements. Therefore, as flat mica sheets as possible were selected as substrates.

Thickness and Morphology: Film thicknesses were measured by X-ray reflectivity (XRR, PANalytical X'Pert Pro MPD or Rigaku SmartLab) or atomic force microscopy (AFM, Veeco Multimode V). For AFM, a step exposing the substrate was created by gently scratching the film with the tip of a needle. For SiO_2/Si, a ≈ 1.8 nm native oxide layer was included in the XRR model, whereas a ≈ 1 nm low-density surface layer on the sapphire surface, as measured from a bare annealed wafer, was necessary to obtain adequate fits to the measured data. Additional thickness measurements were performed using ellipsometry (Film Sense FS1 Multi-wavelength ellipsometer), cross-sectional transmission electron microscopy (TEM, Hitachi HD2700 aberration corrected scanning transmission electron microscope at EAG Laboratories), and LEIS (described below). The TEM sample was prepared by focused ion beam (FIB) lift-out method using a FEI Helios 660 Dual-Beam FIB/SEM instrument.

Film morphology was studied by AFM in tapping mode in air using silicon probes (Bruker) with a nominal tip radius of less than 10 nm. The images were flattened or planefitted to remove measurement artefacts. Film roughness was calculated as a root mean square value (R_q).

Evaluation of Film Coverage: Surface coverages of films deposited on SiO_2/Si and sapphire were determined by low energy ion scattering (LEIS, IONTOF Qtac100) using 3 keV $^4He^+$ ions.[83,84] Samples were cleaned by an exposure to atomic oxygen to remove adventitious organic compounds. It was estimated that one monolayer (0.33 nm) of SnO_2 was formed on top of the SnS_2 film due to the cleaning procedure. Without the cleaning, only the adventitious contaminants (carbon) were observed. Flash heating to 300 °C was tested as an alternative cleaning method, but it turned out to be unreliable with respect to precise and repeatable elemental quantification. We attribute this to physical or chemical changes taking place in the SnS_2 layer at this temperature. However, flash heating removed the organic contaminants and a surface consisting of only Sn and S was revealed. No oxygen was observed, which confirmed that the samples were not oxidized even after storing for two years in a desiccator (dried air). In the films on sapphire, some impurities (F, Na, and K) were detected in amounts that did not correlate with the film thickness. As these elements are commonly observed contaminants, they were attributed to contamination of the samples after the deposition.

The film coverage was calculated by comparing the surface Sn peak height to that measured from a fully closed SnS_2 film deposited using 250 cycles on SiO_2/Si. Full coverage of this sample was confirmed by the disappearance of the substrate Si peak. The 250 cycle sample on sapphire was also assumed to fully cover the substrate despite apparent damage (scratches) on the analyzed surface. In LEIS, signal from sub-surface layers appears as a low-energy tail of the surface peak. The Sn signal from the second SnS_2 layer (first sub-surface layer) was used to distinguish areas of the SnS_2 films with one or multiple layers. One Sn layer detected by LEIS was estimated to correspond to a SnS_2 monolayer, although this assumption has to be treated with caution. Multilayer coverage was obtained by subtracting the surface Sn peak from the data and comparing the intensity (height) of the remaining sub-surface Sn signal to the 250 cycle sample, which was assumed to consist of at least two fully closed monolayers (Figure S13, Supporting Information). Coverage of monolayer areas was then calculated by subtracting the multilayer coverage from the total coverage. Film (island) thickness was estimated from the width of the sub-surface tail, that is, the number of sub-surface layers. The reported thickness represents the average thickness of film areas with at least two SnS_2 layers.

Evaluation of Crystallinity: Film crystallinity was analyzed by XRD (Rigaku SmartLab) using either grazing incidence (ω = 1°), θ–2θ, or in-plane diffraction (2$\theta\chi$ scans, incident angle 0.3°) geometry. The diffractometer was equipped with a non-monochromatized copper X-ray tube mainly emitting Cu Kα radiation (λ ≈ 1.54 Å, consisting of Kα1 at

© 2020 The Authors. Published by Wiley-VCH GmbH

1.5406 Å and Kα2 at 1.5443 Å). Cu Kβ ($\lambda = 1.39$ Å) and W Lα ($\lambda = 1.48$ Å) lines were also present, the latter due to tungsten evaporated from the cathode to the anode in the X-ray tube.

Out-of-plane orientation was studied using ω (rocking curve) and α scans (section of an in-plane pole figure with a fixed, arbitrary β) of the (0001)SnS_2 reflection ($2\theta = 14.8°$). For α scans we define the center of the pole figure representing planes parallel to the substrate surface as $\alpha = 90°$. The α scans provided more details on the orientation of less strongly textured films compared to the conventional ω scans. The in-plane orientation was analyzed by ϕ scans of the (060)mica and $(10\bar{1}0)SnS_2$ in-plane reflections at 61.8° and 28.4° $2\theta\chi$, respectively.

VESTA software[85] was used to visualize the structures of berndtite (1T) SnS_2 (JCPDS-ICDD powder diffraction file (PDF) 26–677) and $2M_1$ muscovite mica (JCPDS-ICDD PDF 72–1503).

Supporting Information

Supporting Information is available from the Wiley Online Library or from the author.

Acknowledgements

The research was supported by ASM Microchemistry. TEM sample preparation and imaging was performed by EAG Laboratories.

Conflict of Interest

The authors declare no conflict of interest.

Keywords

2D materials, atomic layer deposition, semiconductors, SnS_2

Received: June 11, 2020
Published online: August 7, 2020

[1] K. S. Novoselov, A. K. Geim, S. V. Morozov, D. Jiang, Y. Zhang, S. V. Dubonos, I. V. Grigorieva, A. A. Firsov, *Science* **2004**, *306*, 666.
[2] B. Radisavljevic, A. Radenovic, J. Brivio, V. Giacometti, A. Kis, *Nat. Nanotechnol.* **2011**, *6*, 147.
[3] K. Zhang, Y. Feng, F. Wang, Z. Yang, J. Wang, *J. Mater. Chem. C* **2017**, *5*, 11992.
[4] A. H. C. Neto, F. Guinea, N. M. R. Peres, K. S. Novoselov, A. K. Geim, *Rev. Mod. Phys.* **2007**, *81*, 109.
[5] S. Zhao, T. Hotta, T. Koretsune, K. Watanabe, T. Taniguchi, K. Sugawara, T. Takahashi, H. Shinohara, R. Kitaura, *2D Mater.* **2016**, *3*, 025027.
[6] M. Chhowalla, H. S. Shin, G. Eda, L.-J. Li, K. P. Loh, H. Zhang, *Nat. Chem.* **2013**, *5*, 263.
[7] X. Song, Z. Guo, Q. Zhang, P. Zhou, W. Bao, D. W. Zhang, *Small* **2017**, *13*, 1700098.
[8] X. Duan, C. Wang, A. Pan, R. Yu, X. Duan, *Chem. Soc. Rev.* **2015**, *44*, 8859.
[9] F. Schwierz, J. Pezoldt, R. Granzner, *Nanoscale* **2015**, *7*, 8261.
[10] M. Chhowalla, D. Jena, H. Zhang, *Nat. Rev. Mater.* **2016**, *1*, 16052.
[11] M. Akhtar, G. Anderson, R. Zhao, A. Alruqi, J. E. Mroczkowska, G. Sumanasekera, J. B. Jasinski, *npj 2D Mater. Appl.* **2017**, *1*, 5.
[12] Y. Huang, E. Sutter, J. T. Sadowski, M. Cotlet, O. L. A. Monti, D. A. Racke, M. R. Neupane, D. Wickramaratne, R. K. Lake, B. A. Parkinson, P. Sutter, *ACS Nano* **2014**, *8*, 10743.
[13] L. A. Burton, T. J. Whittles, D. Hesp, W. M. Linhart, J. M. Skelton, B. Hou, R. F. Webster, G. O'Dowd, C. Reece, D. Cherns, D. J. Fermin, T. D. Veal, V. R. Dhanak, A. Walsh, *J. Mater. Chem. A* **2016**, *4*, 1312.
[14] X. Zhou, Q. Zhang, L. Gan, H. Li, J. Xiong, T. Zhai, *Adv. Sci.* **2016**, *3*, 1600177.
[15] J. M. Gonzalez, I. I. Oleynik, *Phys. Rev. B – Condens. Matter Mater. Phys.* **2016**, *94*, 125443.
[16] G. Ye, Y. Gong, S. Lei, Y. He, B. Li, X. Zhang, Z. Jin, L. Dong, J. Lou, R. Vajtai, W. Zhou, P. M. Ajayan, *Nano Res.* **2017**, *10*, 2386.
[17] H. S. Song, S. L. Li, L. Gao, Y. Xu, K. Ueno, J. Tang, Y. B. Cheng, K. Tsukagoshi, *Nanoscale* **2013**, *5*, 9666.
[18] L. Xu, H. Jiang, X.Wang, F. C. , Z. Hu, Y. Gong, L. Shang, J. Zhang, K. Jiang, J. Chu, *Small* **2019**, *15*, 1904116.
[19] Y. Gong, H. Yuan, C.-L. Wu, P. Tang, S.-Z. Yang, A. Yang, G. Li, B. Liu, J. van der Groep, M. L. Brongersma, M. F. Chisholm, S.-C. Zhang, W. Zhou, Y. Cui, *Nat. Nanotechnol.* **2018**, *13*, 294.
[20] G. Su, V. G. Hadjiev, P. E. Loya, J. Zhang, S. Lei, S. Maharjan, P. Dong, P. M. Ajayan, J. Lou, H. Peng, *Nano Lett.* **2015**, *15*, 506.
[21] S. Thiele, W. Kinberger, R. Granzner, G. Fiori, F. Schwierz, *Solid State Electron.* **2018**, *143*, 2.
[22] A. Shafique, A. Samad, Y.-H. Shin, *Phys. Chem. Chem. Phys.* **2017**, *19*, 20677.
[23] C. Zhai, N. Du, H. Z. D. Yang, *Chem. Commun.* **2011**, *47*, 1270.
[24] Y. Xie, M. Fan, T. Shen, Q. Liu, Y. Chen, *Mater. Technol.* **2016**, *31*, 646.
[25] J. Z. Ou, W. Ge, B. Carey, T. Daeneke, A. Rotbart, W. Shan, Y. Wang, Z. Fu, A. F. Chrimes, W. Wlodarski, S. P. Russo, Y. X. Li, K. Kalantar-Zadeh, *ACS Nano* **2015**, *9*, 10313.
[26] G. Liu, Y. Qiu, Z. Wang, J. Zhang, X. Chen, M. Dai, D. Jia, Y. Zhou, Z. Li, P. Hu, *ACS Appl. Mater. Interfaces* **2017**, *9*, 37750.
[27] X. Chia, P. Lazar, Z. Sofer, J. Luxa, M. Pumera, *J. Phys. Chem. C* **2016**, *120*, 24098.
[28] G. Liu, Z. Li, T. Hasan, X. Chen, W. Zheng, W. Feng, D. Jia, Y. Zhou, P. Hu, *J. Mater. Chem. A* **2017**, *5*, 1989.
[29] Y. Gao, Z. Liu, D.-M. Sun, L. Huang, L.-P. Ma, L.-C. Yin, T. Ma, Z. Zhang, X.-L. Ma, L.-M. Peng, H.-M. Cheng, W. Ren, *Nat. Commun.* **2015**, *6*, 8569.
[30] Z. Xu, Y. Zhang, S. Lin, C. Zheng, Y. L. Zhong, X. Xia, Z. Li, *ACS Nano* **2015**, *9*, 6178.
[31] A. Castellanos-Gomez, M. Buscema, R. Molenaar, V. Singh, L. Janssen, H. S. J. van der Zant, G. A. Steele, *2D Mater.* **2014**, *1*, 011002.
[32] J.-H. Ahn, M.-J. Lee, H. Heo, J. H. Sung, K. Kim, H. Hwang, M.-H. Jo, *Nano Lett.* **2015**, *15*, 3703.
[33] Y. Hu, T. Chen, X. Wang, L. Ma, R. Chen, H. Zhu, X. Yuan, C. Yan, G. Zhu, H. Lv, J. Liang, Z. Jin, J. Liu, *Nano Res.* **2017**, *10*, 1434.
[34] H. Zhang, T. van Pelt, A. N. Mehta, H. Bender, I. Radu, M. Caymax, W. Vandervorst, A. Delabie, *2D Mater.* **2018**, *5*, 035006.
[35] H. Zhang, Y. Balaji, A. N. Mehta, M. Heyns, M. Caymax, I. Radu, W. Vandervorst, A. Delabie, *J. Mater. Chem. C* **2018**, *6*, 6172.
[36] M. Mattinen, P. J. King, L. Khriachtchev, K. Meinander, J. T. Gibbon, V. R. Dhanak, J. Räisänen, M. Ritala, M. Leskelä, *Small* **2018**, *14*, 1800547.
[37] G. Ham, S. Shin, J. Park, J. Lee, H. Choi, S. Lee, H. Jeon, *RSC Adv.* **2016**, *6*, 54069.
[38] S. Lee, S. Shin, G. Ham, J. Lee, H. Choi, H. Park, H. Jeon, *AIP Adv.* **2017**, *7*, 045307.
[39] N. Lee, G. Lee, H. Choi, H. Park, Y. Choi, H. Seo, H. Ju, S. Kim, O. Sul, J. Lee, S.-B. Lee, H. Jeon, *Nanotechnology* **2019**, *30*, 405707.
[40] J. J. Pyeon, I.-H. Baek, W. C. Lim, K. H. Chae, S. H. Han, G. Y. Lee, S.-H. Baek, J.-S. Kim, J.-W. Choi, T.-M. Chung, J. H. Han, C.-Y. Kang, S. K. Kim, *Nanoscale* **2018**, *10*, 17712.
[41] J. J. Pyeon, I.-H. Baek, W. C. Lee, H. Lee, S. O. Won, G.-Y. Lee, T.-M. Chung, J. H. Han, S.-H. Baek, J.-S. Kim, J.-W. Choi, C.-Y. Kang, S. K. Kim, *ACS Appl. Mater. Interfaces* **2020**, *12*, 2679.

© 2020 The Authors. Published by Wiley-VCH GmbH

[42] M. Ritala, J. Niinistö, in *Chemical Vapour Deposition: Precursors, Processes and Applications* (Eds: A.C. Jones, M. L. Hitchman), Royal Society of Chemistry, Cambridge, UK **2009**, Ch. 4, pp. 158–206.
[43] M. Leskelä, J. Niinistö, M. Ritala, in *Comprehensive Materials Processing*, Vol. *4*, (Eds: S. Hashmi, D. Cameron), Elsevier, Amsterdam, The Netherlands, **2014**, Ch. 5, pp. 101–123.
[44] B. Groven, A. N. Mehta, H. Bender, Q. Smets, J. Meersschaut, A. Franquet, T. Conard, T. Nuytten, P. Verdonck, W. Vandervorst, M. Heyns, I. Radu, M. Caymax, A. Delabie, *J. Vac. Sci. Technol. A* **2018**, *36*, 01A105.
[45] J. Yang, S. Kim, W. Choi, S. H. Park, Y. Jung, M. H. Cho, H. Kim, *ACS Appl. Mater. Interfaces* **2013**, *5*, 4739.
[46] L. Cheng, X. Qin, A. T. Lucero, A. Azcatl, J. Huang, R. M. Wallace, K. Cho, J. Kim, *ACS Appl. Mater. Interfaces* **2014**, *6*, 11834.
[47] B. Groven, M. Heyne, A. N. Mehta, H. Bender, T. Nuytten, J. Meersschaut, T. Conard, P. Verdonck, S. van Elshocht, W. Vandervorst, S. de Gendt, M. Heyns, I. Radu, M. Caymax, A. Delabie, *Chem. Mater.* **2017**, *29*, 2927.
[48] M. Mattinen, T. Hatanpää, T. Sarnet, K. Mizohata, K. Meinander, P. J. King, L. Khriachtchev, J. Räisänen, M. Ritala, M. Leskelä, *Adv. Mater. Interfaces* **2017**, *4*, 1700123.
[49] T. A. Ho, C. Bae, S. Lee, M. Kim, J. M. Montero-Moreno, J. H. Park, H. Shin, *Chem. Mater.* **2017**, *29*, 7604.
[50] Y. Jang, S. Yeo, H.-B.-R. Lee, H. Kim, S.-H. Kim, *Appl. Surf. Sci.* **2016**, *365*, 160.
[51] I.-H. Baek, J. J. Pyeon, Y. G. Song, T.-M. Chung, H.-R. Kim, S.-H. Baek, J.-S. Kim, C.-Y. Kang, J.-W. Choi, C. S. Hwang, J. H. Han, S. K. Kim, *Chem. Mater.* **2017**, *29*, 8100.
[52] J. Hämäläinen, M. Mattinen, K. Mizohata, K. Meinander, M. Vehkamäki, J. Räisänen, M. Ritala, M. Leskelä, *Adv. Mater.* **2018**, *30*, 1703622.
[53] D. H. Kwon, Z. Jin, S. Shin, W.-S. Lee, Y.-S. Min, *Nanoscale* **2016**, *8*, 7180.
[54] D. Xiong, Q. Zhang, W. Li, J. Li, X. Fu, M. F. Cerqueira, P. Alpuim, L. Liu, *Nanoscale* **2017**, *9*, 2711.
[55] L. K. Tan, B. Liu, J. H. Teng, S. Guo, H. Y. Low, K. P. Loh, *Nanoscale* **2014**, *6*, 10584.
[56] T. Jurca, M. J. Moody, A. Henning, J. D. Emery, B. Wang, J. M. Tan, T. L. Lohr, L. J. Lauhon, T. J. Marks, *Angew. Chem. – Int. Ed.* **2017**, *56*, 4991.
[57] B. Groven, A. N. Mehta, H. Bender, J. Meersschaut, T. Nuytten, P. Verdonck, T. Conard, Q. Smets, T. Schram, B. Schoenaers, A. Stesmans, V. Afanas'ev, W. Vandervorst, M. Heyns, M. Caymax, I. Radu, A. Delabie, *Chem. Mater.* **2018**, *30*, 7648.
[58] H. Li, Y. Li, A. Aljarb, Y. Shi, L.-J. Li, *Chem. Rev.* **2018**, *118*, 6134.
[59] A. Koma, *Thin Solid Films* **1992**, *216*, 72.
[60] L. A. Walsh, C. L. Hinkle, *Appl. Mater. Today* **2017**, *9*, 504.
[61] D. Dumcenco, D. Ovchinnikov, K. Marinov, P. Lazic, M. Gibertini, N. Marzari, O. L. Sanchez, Y. Kung, D. Krasnozhon, M. Chen, S. Bertolazzi, P. Gillet, A. Fontcuberta, A. Radenovic, A. Kis, *ACS Nano* **2015**, *9*, 4611.
[62] H. G. Ji, Y.-C. Lin, K. Nagashio, M. Maruyama, P. Solís-Fernández, A. Sukma Aji, V. Panchal, S. Okada, K. Suenaga, H. Ago, *Chem. Mater.* **2018**, *30*, 403.
[63] R. Schlaf, D. Louder, O. Lang, C. Pettenkofer, W. Jaegermann, K. W. Nebesny, P. A. Lee, B. A. Parkinson, N. R. Armstrong, *J. Vac. Sci. Technol., A* **1995**, *13*, 1761.
[64] K. W. Nebesny, G. E. Collins, P. A. Lee, L.-K. Chau, J. Danziger, E. Osburn, N. R. Armstrong, *Chem. Mater.* **1991**, *3*, 829.
[65] R. Schlaf, N. R. Armstrong, B. A. Parkinson, C. Pettenkofer, W. Jaegermann, *Surf. Sci.* **1997**, *385*, 1.
[66] M. Mattinen, P. J. King, G. Popov, J. Hämäläinen, M. J. Heikkilä, M. Leskelä, M. Ritala, *2D Mater.* **2020**, *7*, 011003.
[67] P. R. Ribic, G. Bratina, *Surf. Sci.* **2007**, *601*, 44.
[68] M. Yoshimoto, T. Maeda, T. Ohnishi, H. Koinuma, O. Ishiyama, M. Shinohara, M. Kubo, R. Miura, A. Miyamoto, *Appl. Phys. Lett.* **1995**, *67*, 2615.
[69] A. Aljarb, Z. Cao, H.-L. Tang, J.-K. Huang, M. Li, W. Hu, L. Cavallo, L.-J. Li, *ACS Nano* **2017**, *11*, 9215.
[70] Y.-H. Lee, L. Yu, H. Wang, W. Fang, X. Ling, Y. Shi, C.-T. Lin, J.-K. Huang, M.-T. Chang, C.-S. Chang, M. Dresselhaus, T. Palacios, L.-J. Li, J. Kong, *Nano Lett.* **2013**, *13*, 1852.
[71] H. Ago, H. Endo, P. Solís Fernández, R. Takizawa, Y. Ohta, Y. Fujita, K. Yamamoto, M. Tsuji, *ACS Appl. Mater. Interfaces* **2015**, *7*, 5265.
[72] D. L. Greenaway, R. Nitsche, *Solid State Commun.* **1965**, *3*, 1445.
[73] Y. Bertrand, G. Leveque, C. Raisin, F. Levy, *J. Phys. C Solid State Phys.* **1979**, *12*, 2907.
[74] W. de Poel, S. Pintea, J. Drnec, F. Carla, R. Felici, P. Mulder, J. A. A. W. Elemans, W. J. P. van Enckevort, A. E. Rowan, E. Vlieg, *Surf. Sci.* **2014**, *619*, 19.
[75] F. Ostendorf, C. Schmitz, S. Hirth, A. Kühnle, J. J. Kolodziej, M. Reichling, *Nanotechnology* **2008**, *19*, 305705.
[76] Y. Bitla, Y. H. Chu, *FlatChem* **2017**, *3*, 26.
[77] C. Simbrunner, G. Hernandez-Sosa, M. Oehzelt, T. Djuric, I. Salzmann, M. Brinkmann, G. Schwabegger, I. Watzinger, H. Sitter, R. Resel, *Phys. Rev. B – Condens. Matter Mater. Phys.* **2011**, *83*, 115443.
[78] M. Grundmann, T. Böntgen, M. Lorenz, *Phys. Rev. Lett.* **2010**, *105*, 146102.
[79] J. E. Boschker, L. A. Galves, T. Flissikowski, J. M. J. Lopes, H. Riechert, R. Calarco, *Sci. Rep.* **2016**, *5*, 18079.
[80] D. S. Koda, F. Bechstedt, M. Marques, L. K. Teles, *J. Phys. Chem. C* **2016**, *120*, 10895.
[81] J. Narayan, B. C. Larson, *J. Appl. Phys.* **2003**, *93*, 278.
[82] M. Leskelä, M. Mattinen, M. Ritala, *J. Vac. Sci. Technol. B* **2019**, *37*, 030801.
[83] H. H. Brongersma, M. Draxler, M. de Ridder, P. Bauer, *Surf. Sci. Rep.* **2007**, *62*, 63.
[84] C. V. Cushman, P. Brüner, J. Zakel, G. H. Major, B. M. Lunt, N. J. Smith, T. Grehl, M. R. Linford, *Anal. Methods* **2016**, *8*, 3419.
[85] K. Momma, F. Izumi, *J. Appl. Crystallogr.* **2011**, *44*, 1272.

© 2020 The Authors. Published by Wiley-VCH GmbH